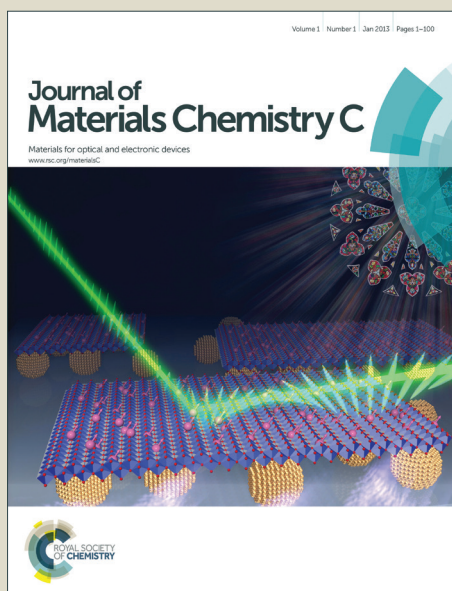


Journal of Materials Chemistry C

Accepted Manuscript



This article can be cited before page numbers have been issued, to do this please use: P. K. P, C. S, K. Krishnamoorthy and A. SK, *J. Mater. Chem. C*, 2014, DOI: 10.1039/C4TC01806K.



This is an *Accepted Manuscript*, which has been through the Royal Society of Chemistry peer review process and has been accepted for publication.

Accepted Manuscripts are published online shortly after acceptance, before technical editing, formatting and proof reading. Using this free service, authors can make their results available to the community, in citable form, before we publish the edited article. We will replace this *Accepted Manuscript* with the edited and formatted *Advance Article* as soon as it is available.

You can find more information about *Accepted Manuscripts* in the [Information for Authors](#).

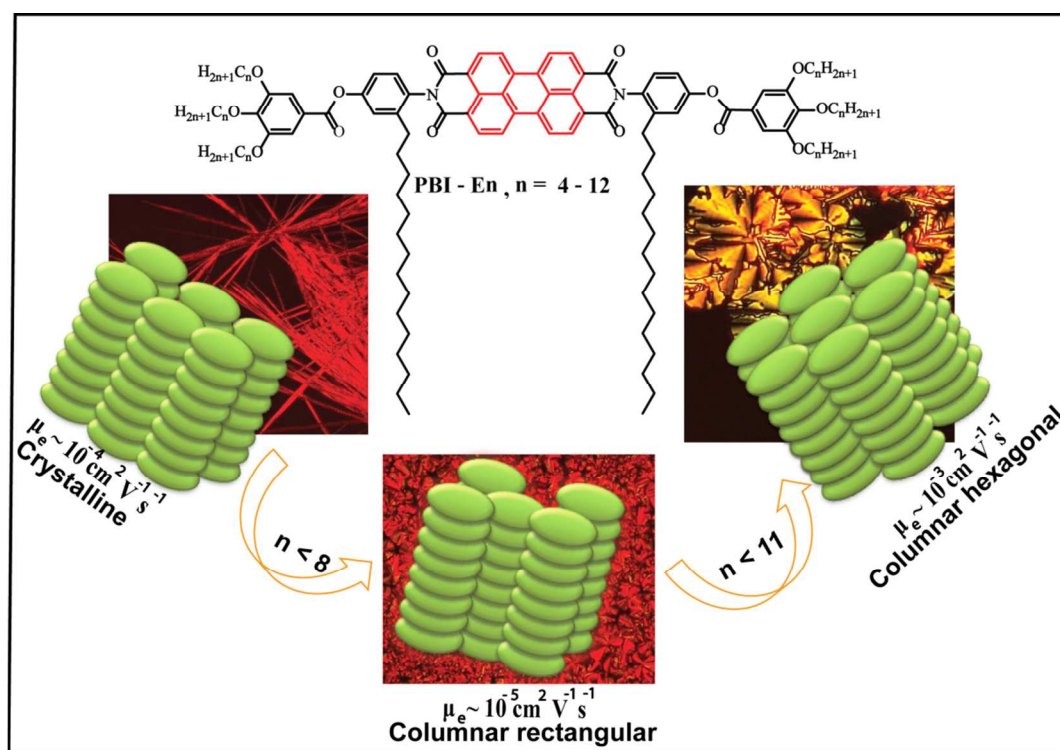
Please note that technical editing may introduce minor changes to the text and/or graphics, which may alter content. The journal's standard [Terms & Conditions](#) and the [Ethical guidelines](#) still apply. In no event shall the Royal Society of Chemistry be held responsible for any errors or omissions in this *Accepted Manuscript* or any consequences arising from the use of any information it contains.

Revised Manuscript submitted to *Journal of Materials Chemistry C*
(Manuscript ID TC-ART-08-2014-001806)

Structure-Property Relationship in Charge Transporting Behaviour of Room Temperature Liquid Crystalline Perylenebisimides.

K. P. Prajitha,^{a,b} S. Chithiravel,^a K. Krishnamoorthy*^{a,b,c} and S. K. Asha*^{a,b,c}

- Polymer Science and Engineering Division, CSIR-National Chemical Laboratory, Dr Homi Bhabha Road, Pune 411008, India.
- Academy of Scientific and Innovative Research, New Delhi, India
- CSIR-Network Institutes of Solar Energy, New Delhi, India



Corresponding Author: S. K. Asha, E-mail: sk.asha@ncl.res.in Fax: 0091-20-25902615.
K. Krishnamoorthy, E-mail: k.krishnamoorthy@ncl.res.in

Abstract:

A homologous series of pentadecyl phenol functionalized perylenebisimide (PBI) terminated with trialkoxy gallate esters were synthesized, where the terminal alkyl chain length was varied from $n = 4$ to 12 (PBI-En). The thermotropic liquid crystalline (LC) characteristics of the molecules were analyzed using differential scanning calorimetry (DSC), polarized light microscopy (PLM) combined with variable temperature wide angle X-ray diffraction (WXR) techniques. A clear odd-even oscillation was observed in the melting as well as isotropization enthalpies as a function of alkyl spacer length in the terminal gallate unit with the even spacers exhibiting higher values. The higher members of the series with $n > 8$ exhibited thermotropic liquid crystalline textures in the PLM which remained stable until room temperature. The nature of the LC phase was identified to be columnar rectangular and columnar hexagonal based on detailed analysis of the WXR pattern recorded in the LC phases. The WXR pattern of the room temperature LC frozen samples indicated a nearly constant intra columnar stack distance of $\sim 3.7 \text{ \AA}$ for all the members. The space charge limited current (SCLC) values of the LC frozen sample films were analyzed for dependence of bulk mobility estimate on the nature of the LC phase. The columnar hexagonal phase exhibited a mobility value one order ($10^{-3} \text{ cm}^2\text{V}^{-1}\text{s}^{-1}$) higher than that of crystalline ($10^{-4} \text{ cm}^2\text{V}^{-1}\text{s}^{-1}$) and two orders higher than that of columnar rectangular phase ($10^{-5} \text{ cm}^2\text{V}^{-1}\text{s}^{-1}$) indicating a strong dependence of packing on bulk mobility.

Introduction

Charge transport in organic semiconducting materials is a very active research area because of their potential applications in optoelectronic materials such as organic field effect transistors (OFET), organic light emitting diodes (OLED), organic photovoltaic cells (OPV) etc.¹⁻⁴ In this perspective columnar liquid crystalline (LC) materials are well recognized because of their ability to self organize in to an ordered architecture allowing for one dimensional charge transport resulting in a high charge carrier mobility.⁵⁻⁸ In the columnar liquid crystals, the disc like mesogens are stacked one on top of another surrounded by the flexible alkyl chain resulting in mesophase formation. The disc like molecules can form stable columns (typical intra columnar distance of 3.5-3.9 Å) due to the strong π - π stacking between the poly aromatic core with significant overlap of p-orbital, which results in effective charge transport.⁹ Upon thermal annealing, these molecules can form single large domain with less number of grain boundaries as a result of their inherent self healing property due to their partial liquid-like behavior.¹⁰⁻¹² Therefore, columnar liquid crystalline materials have several advantages over organic single crystalline materials including easy processing, ability to form thin films, long range self assembly, less number of grain boundaries etc which are the key factors for efficient charge transporting.^{13, 14} But the main challenge in this area is the attainment of mesogenicity in a temperature range that is adaptable on a device substrate.¹⁵ The clearing temperatures should be low and ideally the liquid crystalline phase should be retained at room temperature.

However, the design of a suitable LC material for a desired application requires a basic understanding of the structure-property relationship. Depending on the lateral chain length of the substituent, the inter columnar distance is usually in the range of 20-40 Å. The interactions between the adjacent molecules within the same column is much stronger than the interactions between neighboring columns which results in better one dimensional charge transport. Depending on the extent of core-core packing, the columnar phases can be further classified in to ordered and disordered columnar mesophase.^{8, 9} For device application, columnar ordered phases are preferred because of the effective π - π stacking. Further, depending on the core and spacer interactions the columnar phase can self assemble in to columnar hexagonal, columnar rectangular, columnar oblique, columnar lamellar or columnar plastic mesophases. Among these the columnar hexagonal (Col_h) and columnar

rectangular (Col_r) phases are the two commonly observed mesophases in the discotic systems.^{16, 17} Columnar plastic phase (Col_p) is the highest ordered phase having three dimensional positional order as in crystalline state along with rotational mobility.¹⁸ Because of these characteristics columnar plastic phase has been considered as an ideal charge transporting system and better mobility values have been observed in these systems.¹⁹ Further understanding of packing and charge transport in these systems are required as only few reports are available in literature.^{19, 20}

The liquid crystalline and charge transporting properties of p type semiconducting systems like triphenylenes, phthalocyanin, hexabenzocoronene etc are well studied in literature.²¹⁻²³ However, there are only limited choices as far as n type semiconducting liquid crystalline materials are concerned.^{24, 25} Perylenebisimides (PBI) are an n type organic semiconducting material with inherent mesogenicity possessing high thermal and photo stability along with high absorption coefficient.²⁶ Aromatic π - π stacking, van der waals interaction, hydrogen bonding, chirality etc are some of the major tools that have been reported to self assemble PBI based systems to desired architectures.²⁷ With suitable molecular design, the PBI derivatives can be made to exhibit a wide array of liquid crystalline phases. Struijk et al. reported a linear aliphatic chain substituted liquid crystalline PBI derivative with a mobility of $0.1 \text{ cm}^2 \text{ V}^{-1} \text{ s}^{-1}$ determined by pulse-radiolysis time-resolved microwave conductivity (PR-TMC) method.²⁸ Marder et al. reported liquid crystalline dodecyloxy ester derivative of PBI with a mobility of $1.3 \text{ cm}^2 \text{ V}^{-1} \text{ s}^{-1}$ by SCLC method which is one of the highest charge carrier mobility reported so far in the LC phase.²⁹ Recently, Thelekkat et al. compared the charge carrier mobility in crystalline vs liquid crystalline perylenebisimide and observed that the LC PBI exhibited SCLC mobility of $7 \times 10^{-3} \text{ cm}^2 \text{ V}^{-1} \text{ s}^{-1}$ which was 2 orders higher compared to their crystalline counterpart.³⁰ Similar report has come from the group of Zhang et al., where a liquid crystalline PBI showed high mobility value compared to the crystalline state.³¹

Based on the above evidence from literature, it is clear that the charge transport properties of the PBIs could be fine-tuned by controlling the molecular structure factors that decide the crystalline or liquid crystalline ordering. In this scenario we have undertaken a systematic study on the spacer effect on mesogenic and charge transport properties in a series of 3, 4, 5-tri alkoxy ester derivative of symmetrically substituted pentadecyl phenol based

perylenebisimides. It has been well established that the methylene units in the even spacer can pack efficiently compared to the odd spacers, which is directly reflected in their mesophase behavior as well as phase transitions.³² Previously Percec et al. systematically studied the effect of spacer on the perylenebisimide core and on the terminal spacer in dendritic PBI molecules.^{33, 34} Very recently, Grozema et al. reported systematic study on a series of PBI derivatives terminated with linear alkylester chains where the length of the alkyl chain as well as the position of the ester group on the aliphatic unit was varied and the charge transport characteristics was probed. Mobilities as high as $0.22 \text{ cm}^2 \text{ V}^{-1} \text{ s}^{-1}$ was observed using the PR-TMC technique and results showed that the mobility values could be tuned by varying the relative position of the ester group in the side chain.³⁵

Previously we had reported the liquid crystalline ordering of 3,4,5-tri dodecyloxy substituted pentadecyl phenol based PBI ester which was shown to exhibit room temperature columnar mesophase.³⁶ Taking advantage of the unique self assembling characteristics afforded by the pentadecyl phenol imide substitution on PBI, we have designed a series of PBI derivatives (**PBI-En**; n: 4-12) where the terminal spacer in the alkoxy chain was varied from 4 to 12 for understanding the effect of spacer length on the intrinsic properties. The molecules were structurally characterized and their mesophase characteristics were determined using differential scanning calorimetry (DSC), polarizing light microscope (PLM) and variable temperature wide angle X-ray diffraction (VT-WXRD) studies. The charge transport properties were explored using space charge limited current (SCLC) measurements. The important aspects that were explored in this work are highlighted below.

- 1) A detailed structure-property analysis relating the role of the varying terminal trialkoxy spacer length on the liquid crystalline ordering in the PBI-En series.
- 2) Correlation of the bulk mobility estimate, determined using the SCLC method among the crystalline and different LC phases.

EXPERIMENTAL SECTION

Materials: Perylene-3,4,9,10-tetracarboxylic dianhydride (PTCDA), 3-pentadecyl phenol, zinc acetate, imidazole, methyl-3,4,5-trihydroxybenzoate, triethylamine, 1-bromobutane, 1-bromopentane, 1-bromohexane, 1-bromoheptane, 1-bromooctane, 1-bromononane, 1-bromodecane, 1-bromoundecane and 1-bromododecane were purchased from Sigma-Aldrich and

used without further purification. Sodium nitrite and potassium carbonate were purchased from Merck Chemicals Ltd and used as such. Thionyl chloride, tri-ethyl amine, dimethyl formamide (DMF), dichloromethane (DCM), tetrahydrofuran (THF) and ethanol were purchased from Merck Chemicals Ltd and were purified using standard procedures.

Instrumentation:

$^1\text{H-NMR}$ and $^{13}\text{C-NMR}$ spectra of **PBI-En** molecules were recorded on a Bruker-AVANCE 200 MHz spectrometer. Chemical shifts are reported in ppm at 25 $^{\circ}\text{C}$ using CDCl_3 as solvent containing small amount of tetramethylsilane (TMS) as internal standard. The purity of samples was confirmed using elemental analysis, which was done using a Thermo Finnigan Flash EA 1112 series CHNS analyzer. Gel Permeation Chromatography (GPC) was carried out on Polymer Laboratories PL-GPC-220 using CHCl_3 as eluent. The flow rate of CHCl_3 was maintained as 1 $\mu\text{L}/\text{min}$ throughout the experiments and the sample solutions at concentrations 2-3 mg/ml were filtered through syringe filter and injected for recording the chromatograms at 30 $^{\circ}\text{C}$. The mass spectral analysis was carried out in reflecting mode with an accelerating voltage of 25 kV using a Voyager-De-STRMALDI-TOF (Applied Biosystems, Framingham, MA, USA) instrument equipped with 337 nm pulsed nitrogen laser used for desorption and ionization. The sample was made in CHCl_3 and premixed with dithranol matrix before spotting on 96-well stainless steel MALDI plate by dried droplet method. Infrared spectra were recorded using Bruker FT-IR (ATR mode) spectrophotometer in the range of 4000-600 cm^{-1} . The thermal stability of the PBI-En were analyzed using PerkinElmer STA-6000 thermogravimetric analyser (TGA) under nitrogen atmosphere from 40-800 $^{\circ}\text{C}$ at 10 $^{\circ}\text{C}/\text{min}$. Differential Scanning Calorimetry (DSC) was performed using a TA Q10 model. About 2–3 mg of the samples were taken in aluminium pan, sealed and scanned at 10 $^{\circ}\text{C}/\text{min}$ under nitrogen atmosphere. The instrument was calibrated with indium standards before measurements. The phase behaviour of the molecules was analyzed using LIECA DM2500P polarized optical microscope equipped with Linkam TMS 94 heating and cooling stage connected to a Linkam TMS 600 temperature programmer. The Transition from isotropic to liquid crystalline phase was monitored by the evolution of characteristic textures. X-ray diffraction of all the annealed samples were recorded by a DY 1042-Emprean XRD with Programmable Divergence Slit (PDS) and PIXcel 3D detector using Cu

$K\alpha$ (1.54 Å) emission. The spectra were recorded in the range of (2θ) 2–50° and analyzed using X'pert software. Variable temperature in situ XRD experiments were carried out in an Anton-Paar XRK900 reactor.

Device Fabrication: SCLC electron-only devices were fabricated using the following structure: glass/Al/active layer/Al. The glass substrates were cleaned using the following sequence in an ultrasonic bath: water, acetone, and 2-propanol.³⁷ The bottom aluminum electrode was deposited by thermal evaporation technique with a thickness of 100 nm under vacuum in a glove box. 20 mg/ml of **PBI-En** samples were dissolved in dry chloroform and 70 micro liters was drop cast on top of the aluminum electrode. The drop cast films were annealed above their clearing temperature for 20 minutes and cooled to room temperature. Aluminum counter electrodes were evaporated through a shadow mask on top of the active layer to a thickness of ~100 nm in a thermal evaporation chamber. The active device area was found to be in the range of 0.08 - 0.12 cm². The mobility measurements were carried out by measuring the current–voltage characteristics with a Keithley 2400 source meter.

Results and Discussion

Synthesis and characterization

A series of trialkoxy ester terminated derivatives of perylenebisimide (**PBI-En**; n = 4-12) was designed and developed by esterification reaction between pentadecyl phenol substituted perylenebisimide and 3,4,5-trialkoxo benzoyl chloride. The alkoxy spacer length was varied from 4 to 12 and the synthetic route is shown in scheme-1. The synthesis of the pentadecyl phenol substituted perylenebisimide as well as the 3,4,5-tridodecyloxy substituted PBI molecule, (**PBI-E12**) was described in detail in an earlier report.³⁶ The peripheral 3,4,5-trialkoxo phenyl substitution is known to be helpful in inducing mesogenicity in perylenebisimides, however the long C15 alkyl chain in the ortho position to the imide linkage proved crucial in widening the liquid crystalline window as well as to retain the liquid crystalline order until room temperature. The resulting **PBI-En** molecules were structurally characterized using proton NMR spectroscopy, mass analysis using MALDI-TOF and purity confirmed by single peak in Gel Permeation Chromatography (GPC) as well

as elemental analysis. The proton NMR spectra as well as the other structural characterization data are given in the supporting information (figure S1 to S3).

Mesophase Characteristics of PBI-En

The thermal stability of the **PBI-En** series of molecules was determined by TGA under N₂ atmosphere. Figure S4 shows the TGA curves of the series recorded at a heating rate of 10 °C/min from 40-800 °C. All molecules were observed to be thermally stable up to 370 °C. Table-1 shows the 10 wt % decomposition temperature of the molecules. The thermotropic liquid crystalline characteristics of the **PBI-En** series were studied using differential scanning calorimetry (DSC) analysis coupled with polarized light microscope (PLM) as well as temperature dependant X-ray diffraction (VTXRD). Most of the molecules exhibited multiple transitions both in the heating and cooling cycles. Figure 1 shows the DSC second heating and cooling scans of the entire series and the transition temperatures and corresponding enthalpies in the cooling cycle are summarized and given in table-1. **PBI-E4** exhibited two transitions both in the heating (22 °C, 1.99 kJ/mol; 264.4 °C, 71.86 kJ/mol) as well as cooling cycle (21.05 °C, 2.06 kJ/mol; 250.5 °C, 71.43 kJ/mol). Multiple transitions (more than two) were observed in the case of almost all other molecules in the series. Figure 2a shows the plot of the transition enthalpies for the clearing (while heating) and the crystallization (while cooling) transitions as a function of the number of carbon atoms in the terminal alkoxy spacer length. An interesting odd-even oscillation could be observed in the change in enthalpy (ΔH), with the even members exhibiting higher values as a function of the number of carbon atom in the terminal alkoxy spacer segment. The clearing and the crystallization temperature were also plotted as a function of the number of carbon atom in the terminal alkoxy spacer segment (figure 2b). A weak odd-even oscillation with a steady decrease in the transition temperature was observed as the spacer length increased from 4 to 9; thereafter a strong odd-even oscillation was observed for members 9 to 12. It is a well studied and understood concept that the even spacer can pack more efficiently compared to the odd one. The highly packed structure requires more energy for melting (endothermic) and similarly releases more energy (exothermic) while crystallizing as compared to the weakly packed molecules. This is reflected in the clearing transitions as well as entropies and enthalpy values. The enthalpy of clearing transitions was almost equal to the first transition from

isotropic to crystalline / liquid crystalline phase, which indicated a thermodynamically stable phase rather than a kinetically driven one.³⁴ Although odd-even oscillation in transition temperature has been reported for a variety of mesogens like azobenzene,³⁸ biphenyl,^{39, 40} and oligo phenylene vinylenes,⁴¹ there has so far been no reports on similar observation in the perylenebisimide chromophores.

The phase identification of the various transitions observed in the DSC thermogram was carried out using Polarized Light Microscopic (PLM) analysis enabled with a programmable hot stage. The experimental procedure involved placing a trace amount of the sample on a cover glass plate, heating to melt at 10 °C/min, holding at isotropic state (10 °C higher than the clearing temperature) for 10 minutes followed by slow cooling of 5 °C/ min. The images captured at various temperature intervals are shown in figure S6. Figure 3 shows the texture retained at room temperature for all the samples. Although two transitions were observed both in heating and cooling cycle for **PBI-E4**, the transition at 250.5 °C while cooling corresponded to crystallization and that at 264 °C while heating was the clearing transition. A fast crystallization with growth of sharp needle like textures which remained until room temperature, confirmed the crystalline nature for **PBI-E4**. Similarly, **PBI-E5**, **PBI-E6** and **PBI-E7** also exhibited fast crystallization upon cooling from the isotropic melt which confirmed the absence of liquid crystallinity in these samples. **PBI-E8** formed lancet-like textures upon cooling from isotropic state to 212 °C. These were characteristic columnar textures and it remained unchanged until room temperature. **PBI-E9** exhibited clearing transition at 202 °C; upon cooling from the isotropic melt it exhibited a characteristic snowflake like texture identified as columnar mesophase at 190 °C. Upon slow cooling to 180 °C the domain size seemed to increase. In the DSC cooling cycle also a clearly distinguishable transition was observed around this temperature, indicating a phase transition. The columnar mesophase texture remained stable until room temperature (25 °C). The transitions observed during cooling could be attributed to a columnar disordered to a columnar ordered one. In all cases, the transition observed below room temperature in the DSC (which could not be traced under PLM), could be the reorganization of the alkyl segments.⁴² **PBI-E10** exhibited beautiful leaf-like textures at 213 °C upon cooling from the isotropic melt which remained stable until room temperature. Similarly **PBI-E11** also had a clearing point at 200 °C during heating which on cooling formed the leaf-like textures at 192 °C. The mesophase

characterization of **PBI-E12** was reported previously.³⁶ In short, it had a clearing point at 215 °C and upon cooling snow flake like textures appeared at 200 °C corresponding to columnar hexagonal disordered phase. Further cooling resulted in a large dendritic growth corresponding to formation of columnar ordered phase. Thus, based on the observation under the PLM it could be concluded that the PBI-En molecules with shorter terminal spacer exhibited a tendency to crystallize while those with longer spacer length exhibited typical columnar mesophases upon cooling from the isotropic melt.

Wide angle X-ray diffraction (WXR) analysis of the liquid crystalline phase

The phase identification of the **PBI-En** series was undertaken with the help of wide angle X-ray diffraction (WXR) studies from $2\theta = 2-35^\circ$. The details of the analysis of the WXR pattern of **PBI-E12** were provided in our earlier report.³⁶ In short, a sharp reflection at $2\theta = 2.09^\circ$ having a d spacing of 42.19 Å was indexed as the d_{100} reflection. The other peaks which followed the characteristic ratios of $1:1/\sqrt{4}:1/\sqrt{7}:1/\sqrt{12}$ were indexed as the (100), (200), (210), (220) reflections of the hexagonal lattice. Variable temperature wide angle X-ray diffraction (VT-WXR) studies were undertaken for the samples **PBI-E8**, **PBI-E9**, **PBI-E10** and **PBI-E11** and are given in Figure 4a-d. Figure 4a shows that no reflections were observed for **PBI-E8** in the isotropic state at 235 °C. Around 212 °C, sharp reflections appeared at 2θ values of 2.45° , 5.28° and 5.63° followed by small intense reflections in the 2θ range from 5° - 22° . The DSC thermogram had also indicated a transition at 212.6 °C, which was supported by the observation of lancet like patterns under PLM around 212 °C. Further cooling of the sample resulted in more sharp reflections and shift in peak positions, especially for reflections at 5.28° , and 5.63° and at $2\theta = 21.24^\circ$. The sharp reflection at $2\theta = 2.45^\circ$ having a d spacing of 35.12 Å was indexed as the d_{100} reflection.³⁶ In **PBI-E12** a reflection at $2\theta = 5.35^\circ$ was indexed as the (200) plane. However in **PBI-E8** the reflection around $2\theta = 5^\circ$ was split into two equal intense reflections at 5.28° , and 5.63° which is characteristic of a columnar rectangular phase.²⁰ A similar split was observed for the reflection around $2\theta = 5.5^\circ$ for **PBI-E9**, **PBI-E10** and **PBI-E11** also, which indicated that all of them belonged to the same columnar rectangular phase (the supporting figure S7 compares the expanded 2θ region from 5 to 10° for **PBI-E12** and **PBI-E11** highlighting the split of the peak around $2\theta = 5.5^\circ$). Table-2 shows the temperature and the corresponding d spacing of

peaks which followed the characteristic pattern of a columnar rectangular organization (a ratio of $\cong 1: 4/2: 5/2$ for the d spacing) which was in good agreement with the reported ratio.²⁰ The reflection at $2\theta = 21.24^\circ$ (4.18 Å) and $2\theta = 21.46^\circ$ (4.14 Å) corresponded to the π - π stacking of the perylene core. Upon cooling a gradual shift was observed in the π stacking peaks to higher theta region. At room temperature (25 °C) the π - π stack distance reduced to 3.7 Å (from 4.1 at 230 °C), indicating strong overlapping of the aromatic core. A split due to diffraction from two separate planes was observed in the π stacking reflection around 3.7 Å, which was a characteristic signature of the columnar plastic phase. The splitting indicated better packing in these systems.¹⁸ Plastic phase is characterized by higher crystallinity along with fluidity. Similar VTWXR D studies conducted for the other higher member samples also revealed some common trends. No shift was observed in the d_{100} reflection as a function of temperature, however regular shifts to higher 2θ values were observed for the double reflections around 5.28° and 5.63° as well as for the reflection around $2\theta = 21.24^\circ$ corresponding to the π - π stacking of the perylene aromatic core (inset expanded plot $2\theta = 6.5^\circ - 30^\circ$ in figure 4a-d). In contrast to the appearance of the plastic phase at higher temperature observed in the case of **PBI-E8**, the higher spacer samples like **PBI-E9**, **PBI-E10**, and **PBI-E11** exhibited a split of the π - π stacking reflection around $2\theta = 21.46^\circ$ (4.14 Å) only upon cooling to room temperature. Another striking difference in behavior exhibited by the odd membered samples like **PBI-E9** and **PBI-E11** in comparison with their even membered analogues was the formation of an initial disordered phase at high temperature characterized by absence of the columnar π - π stacking (see the supporting figure S8) this was clearly observed in the DSC thermogram also during the cooling cycle for **PBI-E9**. The cooling cycle in the DSC thermogram of **PBI-E9** (figure 1b) had two exothermic transitions at 191.38 °C (9.37 kJ/mol) and 181.4 °C (3.76 kJ/mol) – the first one corresponding to the isotropic- disordered columnar rectangular phase and the second transition at 181 corresponding to the transition of the disordered phase to a more ordered columnar one. The reflection for the π - π stacking interaction became prominent in the WXR D pattern only below 180 °C. **PBI-E11** also exhibited a similar trend, although the disordered to ordered transition was observed only as a shoulder in the DSC thermogram. Even after carrying out the DSC scan at a cooling rate of 1° C/minute, the shoulder could not

be resolved into a separate peak (supporting figure S5). However, the variable temperature WXRd pattern of **PBI-E11** clearly showed the absence of the peak corresponding to π - π stacking at higher temperature (~ 190 °C); and it appeared while cooling to 180 °C. Thus, it could be confirmed that **PBI-E11** also had the disordered to ordered transition at a high temperature following a similar trend as that of **PBI-E9**. Figure 5 compares the room temperature WXRd data of all the samples in the 2θ range $5^\circ - 30^\circ$ collected after heating to isotropic followed by cooling. It could be seen from the figure that irrespective of the terminal spacer length, the π - π stacking distance was same for all the samples at 3.7 Å. On the other hand, a regular increase was observed in the d spacing for the d_{100} reflection as the number of carbon atoms in the terminal spacer increased (figure S9). The lower homologues **PBI-E4**, **PBI-E5**, **PBI-E6** and **PBI-E7** did not exhibit any liquid crystalline textures as explained earlier; however they also showed a tendency to form columnar stacks as observable from figure S10. Thus the entire series from spacer 4 to spacer 12 could be classified into 3 groups – a lower member group **PBI-E4** to **PBI-E7** which did not exhibit mesophase, a middle spacer series from **PBI-E8** to **PBI-E11** ordered columnar plastic phases and the highest member **PBI-E12** which formed hexagonal ordered columnar phase.

SCLC mobility measurements

SCLC measurement is preferred over the FET measurement due to the stacking of the molecule parallel to the substrate. Therefore, the charge transport is expected to be perpendicular to the substrate. The electron transport characteristics of all members of the **PBI-En** series were investigated by space-charge-limited current (SCLC) method. This method allows for determination of the macroscopic bulk mobility of a material in thin film. The semiconducting PBIs were sandwiched between an electron injecting Aluminum electrode as top and bottom contact with a configuration of glass/Al/**PBI-En**/Al. Aluminum electrodes were chosen for the electron only devices due to the work function (4.3 eV) match with the LUMO of perylenebisimides.⁴³ The samples were heated to isotropic and then cooled to room temperature (25 °C), following which the top Al electrode was deposited. The charge carrier mobilities were evaluated by the current – voltage (I-V) measurement under inert gas atmosphere. The J-V curves present two regimes i) at low voltages; ohmic region where the current measured is potentially limited by the charge traps and a linear relation between J and

V exists; ii) at high voltages; SCLC region where the charge transport is through bulk with less number of traps and $J \propto V^2$. The slope of the region was determined from the log-log J-V plot. The charge carrier mobility was calculated from the slope 2 region, which was determined from the logarithmic plot. The charge carrier mobility in this SCLC region can be calculated from the J-V curve by using Mott-Gurney equation:⁴⁴

$$J = \frac{9}{8} \epsilon_r \epsilon_0 \mu \frac{V^2}{L^3}$$

Where J is the current density, ϵ_r is the dielectric constant of the organic semiconductor (assumed to be 3 in our calculations),⁴⁵ ϵ_0 is the permittivity of free space, μ is the charge carrier mobility, L is the thickness of the active layer, and V is the applied voltage across the device. The SCLC mobility was measured for 5 devices each, the active layer thickness ranged from 5-14 μm (determined using optical profilometer), and covered an area of $\sim 0.08 - 0.12 \text{ cm}^2$. J-V characteristics of annealed films of **PBI-E n** together with the respective fits according to the Mott-Gurney equation are shown in Figure 6. The short spaced ($n < 8$) crystalline molecules exhibited a mobility in the order of $10^{-4} \text{ cm}^2 \text{ V}^{-1} \text{ s}^{-1}$, where as the middle spaced ($n = 8$ to 11) columnar rectangular phase showed mobility in the range of $10^{-5} \text{ cm}^2 \text{ V}^{-1} \text{ s}^{-1}$. The electron mobility value for the columnar hexagonal phase of **PBI-E12** ($n = 12$) was obtained as $2.02 \times 10^{-3} \text{ cm}^2 \text{ V}^{-1} \text{ s}^{-1}$, which was two orders of magnitude higher compared to the other liquid crystalline analogues. This was the highest value observed among the series. The WXR and PLM studies had indicated that **PBI-E12** assembled in the plastic columnar hexagonal phase upon cooling from the isotropic phase. The higher order with flexibility which is a characteristic of the plastic LC phase supported better electron mobility in PBI-E12 compared to the samples assembled in the columnar rectangular phase.¹⁹

Although it was anticipated that the packing difference between the odd and even spaced PBI derivatives would be reflected in their mobility values also, we observed that the bulk mobility estimate was largely influenced by the similar morphologies and crystallinity. The impact of odd-even effect on charge carrier mobility would be pronounced if all the molecules formed similar morphologies and crystallinity. In LC systems, the morphologies and crystallinity were different as a function of alkyl chain length, hence comparison was not straightforward. This was corroborated by the fact that the charge carrier mobility was found to vary by few orders when the crystallinity and morphology varied among the different

members. Thus, the highest SCLC mobility was exhibited by **PBI-E12**, in the columnar hexagonal phase ($10^{-3} \text{ cm}^2 \text{ V}^{-1} \text{ s}^{-1}$), followed by the crystalline molecules **PBI-E4** to **PBI-E7** ($10^{-4} \text{ cm}^2 \text{ V}^{-1} \text{ s}^{-1}$), and the lowest mobility was observed for the **PBI-En** ($n = 8$ to 11) in the columnar rectangular phase ($10^{-5} \text{ cm}^2 \text{ V}^{-1} \text{ s}^{-1}$) indicating a strong dependence of packing on bulk mobility.

Conclusion

A systematic study of the effect of molecular packing on the n-type charge transport characteristics in a novel series of highly soluble pentadecyl phenol substituted perylenebisimide ester derivatives was presented. The homologous **PBI-En** series constituted a 3, 4, 5-tri alkoxy ester derivative of a symmetrical pentadecyl phenol substituted perylenebisimide, where the terminal alkyl spacer length was varied from $n = 4$ to 12 . Detailed characterization using DSC, PLM and variable temperature WXR D established that the members of the homologous series with $n > 8$ exhibited columnar liquid crystalline phases at higher temperature and froze into a columnar plastic phase at room temperature as evidenced by the split appearance of the π - π stacking reflection around $2\theta = 22^\circ$. The lower members of the series with $n < 8$ were crystalline in nature. The PBI derivative with the longest spacer length $n = 12$ (**PBI-E12**) formed columnar hexagonal phase characterized by beautiful dendritic textures under the PLM. The enthalpy of the clearing and crystallization transitions exhibited a strong odd-even oscillation as a function of the number of carbon atoms in the terminal alkoxy unit. The even members exhibited higher enthalpy values due to the more efficient packing of the even membered alkyl spacers in the solid state compared to the odd ones. The bulk mobility of the molecules of the series annealed from the isotropic melt was estimated by the SCLC method using the device configuration of glass/Al/**PBI-En**/Al. The crystalline members with $n < 8$ gave a bulk mobility estimate in the order of $10^{-4} \text{ cm}^2 \text{ V}^{-1} \text{ s}^{-1}$ while the intermediate spacers with $n = 8$ to 11 showed mobility in the range of $10^{-5} \text{ cm}^2 \text{ V}^{-1} \text{ s}^{-1}$ only. A high mobility estimate of $2.02 \times 10^{-3} \text{ cm}^2 \text{ V}^{-1} \text{ s}^{-1}$ was observed for **PBI-E12**, which indicated the direct relation between charge transport and appropriate molecular ordering with better core packing. The liquid-like flexibility combined with the better core packing of the columnar hexagonal plastic phase facilitated slightly better charge transport compared to the three dimensional crystalline packing. The present study thus

highlighted (a) the important role played by the flexible alkyl chains in fine tuning the mesophases in a homologous series of PBI derivatives functionalized with pentadecyl phenol and trialkoxy gallate terminal units. The rigid-flexible balance required for the observation of mesogenicity was attained beyond a terminal alkoxy spacer length of 8 methylene units. The C15 alkyl chain on the pentadecyl phenol unit incorporated into the PBI molecular design also had a crucial role in shaping the liquid crystalline characteristics as well as packing in this series of **PBI-En** molecules. The second highlight of the study was the (b) correlation of the bulk mobility estimate among the different LC and crystalline phases. The SCLC mobility analysis clearly brought out the importance of molecular structural factors that are to be taken into consideration while designing materials for better charge transport.

Acknowledgment:

We thank the DST Nano Mission project SR/NM/NS-1028/2012 and CSIR network project NWP054 for financial support. The authors sincerely thank Professor V. A. Raghunathan and Mrs. Vasudha. K. N., from Raman Research Institute (RRI) Bangalore for variable temperature XRD measurements. Prajitha thanks CSIR-New Delhi, India, for Senior Research Fellowship.

Supporting Information:

Synthetic details for PBI-En molecules, ¹H-NMR spectra, MALDI-TOF, Gel permeation chromatogram (GPC), Thermo gravimetric analysis (TGA) of all PBI-En molecules; PLM images of liquid crystalline **PBI-En** molecules; Room temperature XRD of crystalline **PBI-En** molecules; d spacing and variation of d spacing with spacer length for all the **PBI-En** molecules.

References

- 1 H. Sirringhaus, *Adv. Mater.*, 2005, 17, 2411.
- 2 S. Günes, H. Neugebauer and N. S. Sariciftci, *Chem. Rev.*, 2007, 107, 1324.
- 3 C. Wang, H. Dong, W. Hu, Y. Liu and D. Zhu, *Chem. Rev.*, 2012, 112, 2208.
- 4 Z. Jiang, Z. Zhong, S. Xue, Y. Zhou, Y. Meng, Z. Hu, N. Ai, J. Wang, L. Wang, J. Peng, Y. Ma, J. Pei, J. Wang and Y. Cao, *ACS Appl. Mater. Interfaces*, 2014, 6, 8345.
- 5 L. Schmidt-Mende, A. Fechtenkötter, K. Müllen, E. Moons, R. H. Friend and J. D. MacKenzie, *Science*, 2001, 293, 1119.
- 6 M. Yoshio, T. Mukai, H. Ohno and T. Kato, *J. Am. Chem. Soc.*, 2004, 126, 994.
- 7 N. Boden, R. J. Bushby, J. Clements and B. Movaghar, *J. Mater. Chem.*, 1999, 9, 2081.
- 8 S. Sergeev, W. Pisula and Y. H. Geerts, *Chem. Soc. Rev.*, 2007, 36, 1902-1929.
- 9 S. Kumar, *Chem. Soc. Rev.*, 2006, 35, 83.
- 10 A. J. J. M. van Breemen, P. T. Herwig, C. H. T. Chlon, J. Sweelssen, H. F. M. Schoo, S. Setayesh, W. M. Hardeman, C. A. Martin, D. M. de Leeuw, J. J. P. Valetton, C. W. M. Bastiaansen, D. J. Broer, A. R. Popa-Merticaru and S. C. J. Meskers, *J. Am. Chem. Soc.*, 2006, 128, 2336.
- 11 S. Leng, L. H. Chan, J. Jing, J. Hu, R. M. Moustafa, R. M. Van Horn, M. J. Graham, B. Sun, M. Zhu, K.-U. Jeong, B. R. Kaafarani, W. Zhang, F. W. Harris and S. Z. D. Cheng, *Soft Matter*, 2010, 6, 100.
- 12 J. Eccher, G. C. Faria, H. Bock, H. von Seggern and I. H. Bechtold, *ACS Appl. Mater. Interfaces*, 2014, 5, 11935.
- 13 D. Adam, P. Schuhmacher, J. Simmerer, L. Häussling, K. Siemensmeyer, K. H. Eitzbachi, H. Ringsdorf and D. Haarer, *Nature*, 1994, 371, 141.
- 14 I. McCulloch, M. Heeney, C. Bailey, K. Genevicius, I. MacDonald, M. Shkunov, D. Sparrowe, S. Tierney, R. Wagner, W. Zhang, M. L. Chabynyc, R. J. Kline, M. D. McGehee and M. F. Toney, *Nat. Mater.*, 2006, 5, 328.
- 15 M. Funahashi and A. Sonoda, *J. Mater. Chem.*, 2012, 22, 25190.
- 16 D. Demus, J. Goodby, G. W. Gray, H. W. Spiess and V. Vill, in *Handbook of Liquid Crystals Set*, Wiley-VCH, Verlag GmbH, 2008.
- 17 C. Destrade, N. H. Tinh, H. Gasparoux, J. Malthete and A. M. Levelut, *Mol. Cryst. Liq. Cryst.*, 1981, 71, 111.

- 18 B. Glösen, W. Heitz, A. Kettner and J. H. Wendorff, *Liq. Cryst.*, 1996, 20, 627.
- 19 J. Simmerer, B. Glösen, W. Paulus, A. Kettner, P. Schuhmacher, D. Adam, K.-H. Eitzbach, K. Siemensmeyer, J. H. Wendorff, H. Ringsdorf and D. Haarer, *Adv. Mater.*, 1996, 8, 815.
- 20 Y. Wang, C. Zhang, H. Wu and J. Pu, *J. Mater. Chem. C*, 2014, 2, 1667.
- 21 M. O'Neill and S. M. Kelly, *Adv. Mater.*, 2003, 15, 1135.
- 22 W. Pisula, M. Kastler, D. Wasserfallen, T. Pakula and K. Müllen, *J. Am. Chem. Soc.*, 2004, 126, 8074.
- 23 S. Sergeev, E. Pouzet, O. Debever, J. Levin, J. Gierschner, J. Cornil, R. Gómez Aspe and Y. H. Geerts, *J. Mater. Chem.*, 2007, 17, 1777.
- 24 Y. Dienes, M. Eggenstein, T. Kárpáti, T. C. Sutherland, L. Nyulászi and T. Baumgartner, *Chem. Eur. J.*, 2008, 14, 9878.
- 25 B. A. Jones, A. Facchetti, M. R. Wasielewski and T. J. Marks, *J. Am. Chem. Soc.*, 2007, 129, 15259.
- 26 F. Würthner, *Chem. Commun.*, 2004, 14, 1564.
- 27 A. Wicklein, A. Lang, M. Muth and M. Thelakkat, *J. Am. Chem. Soc.*, 2009, 131, 14442.
- 28 C. W. Struijk, A. B. Sieval, J. E. J. Dakhorst, M. van Dijk, P. Kimkes, R. B. M. Koehorst, H. Donker, T. J. Schaafsma, S. J. Picken, A. M. van de Craats, J. M. Warman, H. Zuilhof and E. J. R. Sudhölter, *J. Am. Chem. Soc.*, 2000, 122, 11057.
- 29 Z. An, J. Yu, S. C. Jones, S. Barlow, S. Yoo, B. Domercq, P. Prins, L. D. A. Siebbeles, B. Kippelen and S. R. Marder, *Adv. Mater.*, 2005, 17, 2580.
- 30 M.-A. Muth, G. Gupta, A. Wicklein, M. Carrasco-Orozco, T. Thurn-Albrecht and M. Thelakkat, *J. Phys. Chem. C*, 2014, 118, 92.
- 31 Y. Zhang, H. Wang, Y. Xiao, L. Wang, D. Shi and C. Cheng, *ACS Appl. Mater. Interfaces*, 2014, 5, 11093.
- 32 C. T. Imrie and P. A. Henderson, *Chem. Soc. Rev.*, 2007, 36, 2096.
- 33 V. Percec, S. D. Hudson, M. Peterca, P. Leowanawat, E. Aqad, R. Graf, H. W. Spiess, X. Zeng, G. Ungar and P. A. Heiney, *J. Am. Chem. Soc.*, 2011, 133, 18479.
- 34 V. Percec, H.-J. Sun, P. Leowanawat, M. Peterca, R. Graf, H. W. Spiess, X. Zeng, G. Ungar and P. A. Heiney, *J. Am. Chem. Soc.*, 2013, 135, 4129.
- 35 D. D. Günbas, C. Xue, S. Patwardhan, M. C. Fravventura, H. Zhang, W. F. Jager, E. J. R.

- Sudhölter, L. D. A. Siebbeles, T. J. Savenije, S. Jin and F. C. Grozema, *Chem. Commun.*, 2014, 50, 4955.
- 36 G. A. Bhavsar and S. K. Asha, *Chem. Eur. J.*, 2011, 17, 12646.
- 37 A. Arulkashmir, B. Jain, J. C. John, K. Roy and K. Krishnamoorthy, *Chem. Commun.*, 2013, 50, 326.
- 38 T. Kobayashi and T. Seki, *Langmuir*, 2003, 19, 9297.
- 39 E. Białecka-Florjańczyk, I. Śledzińska, E. Górecka and J. Przedmojski, *Liq. Cryst.*, 2008, 35, 401.
- 40 S. Kurihara, T. Ikeda and S. Tazuke, *Macromolecules*, 1993, 26, 1590.
- 41 M. Goel and M. Jayakannan, *J. Phys. Chem. B*, 2010, 114, 12508.
- 42 D.-Y. Kim, S.-A. Lee, Y.-J. Choi, S.-H. Hwang, S.-W. Kuo, C. Nah, M.-H. Lee and K.-U. Jeong, *Chem. Eur. J.*, 2014, 20, 5689.
- 43 R. Narayan, P. Kumar, K. S. Narayan and S. K. Asha, *J. Mater. Chem. C*, 2014, 2, 6511-.
- 44 L. Bozano, S. A. Carter, J. C. Scott, G. G. Malliaras and P. J. Brock, *Appl. Phys. Lett.*, 1999, 74, 1132.
- 45 C. Goh, R. J. Kline, M. D. McGehee, E. N. Kadnikova and J. M. J. Fréchet, *Appl. Phys. Lett.*, 2005, 86, 122110.

Table 1. Transition temperature and corresponding enthalpies of **PBI-En** molecules during the second heating and cooling cycles.

Name	T_{cl}^a ($^{\circ}C$) (Lc/C-I)	ΔH_{cl}^a (KJ/mol)	T_c^b ($^{\circ}C$) I-Lc/C	ΔH_c^b (KJ/mol)	T_c^b ($^{\circ}C$) (Lc-C) /(C-C)	ΔH_c^b (KJ/mol)	T_D^c ($^{\circ}C$)
PBI-E4	264	72.83	251	53.17	10	3.81	379
PBI-E5	244	37.46	231	35.10	6	6.28	375
PBI-E6	239	48.23	230	48.68	47	1.23	372
PBI-E7	227	39.8	215	38.64	-6	13.65	376
PBI-E8	221	44.82	212	46.16	-12.7	17.76	376
PBI-E9	202	33.22	191	31.08	10	34.91	370
PBI-E10	212	43.58	205	42	-2.64	23	373
PBI-E11	200	29.17	192	28.17	-8	16.65	372
PBI-E12	215	16.72	202	15.31	13	52.55	370

^a clearing transition and corresponding enthalpy values during heating cycle, ^b phase transitions and corresponding enthalpy values during cooling cycles, ^c 10 % weight loss under N₂ atmosphere during TGA.

Table 2. d-spacing values and phase behavior of the Liquid crystalline **PBI-En** molecules at various temperatures.

Sample	Temperature and d-spacing (Å)					
	230 (⁰ C)	211 (⁰ C)	196 (⁰ C)	175 (⁰ C)	100 (⁰ C)	25 (⁰ C)
PBI – E8	35.92	35.94	35.97	35.99	36.00	36.12
	16.17	16.45	16.21	15.98	15.52	15.43
	15.72	15.49	15.27	15.64	14.77	14.57
	4.17	4.12	4.10	4.05	3.93	3.81
	4.13	4.07	4.05	4.01	3.90	3.72
	Col _{rp}	Col _{rp}	Col _{rp}	Col _{rp}	Col _{rp}	Col _{rp}
PBI – E9	190 (⁰ C)	175 (⁰ C)	100 (⁰ C)	75 (⁰ C)	25 (⁰ C)	
	38.49	38.52	38.54	38.56	38.58	
	16.8	16.45	16.20	15.64	14.89	
	15.88	15.73	15.57	14.98	14.53	
	Col _{rd}	4.15	4.09	4.05	3.82	
PBI- E10	190 (⁰ C)	160 (⁰ C)	130 (⁰ C)	25 (⁰ C)		
	39.98	40.01	40.03	40.07		
	17.54	17.44	17.12	15.27		
	16.80	16.75	16.48	15.14		
	4.3	4.13	4.05	3.81		
PBI- E11	191 (⁰ C)	183 (⁰ C)	127 (⁰ C)	149 (⁰ C)	25 (⁰ C)	
	40.97	41.03	41.06	41.1	41.13	
	16.71	16.54	16.04	16	15.41	
	16.20	15.96	15.27	15.47	15.12	
	Col _{rd}	4.12	4.03	4.01	3.8	
	Col _{ro}	4.01	3.9	3.7		
		Col _{rp}	Col _{rp}	Col _{rp}		

Note: Col_{rp} - columnar rectangular plastic phase, Col_{rd} - columnar rectangular disordered phase and Col_{ro} - columnar rectangular ordered phase.

Table 3. Maximum and average SCLC mobilities of the annealed **PBI-E_n** series of molecules.

Sample	Maximum mobility $\mu_e \text{ max (cm}^2/\text{Vs)}$	Average mobility $\mu_e \text{ Avg (cm}^2/\text{Vs)}$	Mean deviation
PBI-E4	3.35×10^{-4}	2×10^{-4}	$\pm 0.85 \times 10^{-4}$
PBI-E5	8.9×10^{-4}	8.5×10^{-4}	$\pm 2.65 \times 10^{-4}$
PBI-E6	1.7×10^{-4}	1.2×10^{-4}	$\pm 0.40 \times 10^{-4}$
PBI-E7	3.01×10^{-4}	1.81×10^{-4}	$\pm 0.67 \times 10^{-4}$
PBI-E8	3.65×10^{-5}	1.85×10^{-5}	$\pm 1.82 \times 10^{-5}$
PBI-E9	5.65×10^{-5}	2.05×10^{-5}	$\pm 2.05 \times 10^{-5}$
PBI-E10	3.35×10^{-5}	1.81×10^{-5}	$\pm 1.81 \times 10^{-5}$
PBI-E11	4.45×10^{-5}	3.6×10^{-5}	$\pm 1.24 \times 10^{-5}$
PBI-E12	3.67×10^{-3}	2.02×10^{-3}	$\pm 0.67 \times 10^{-3}$

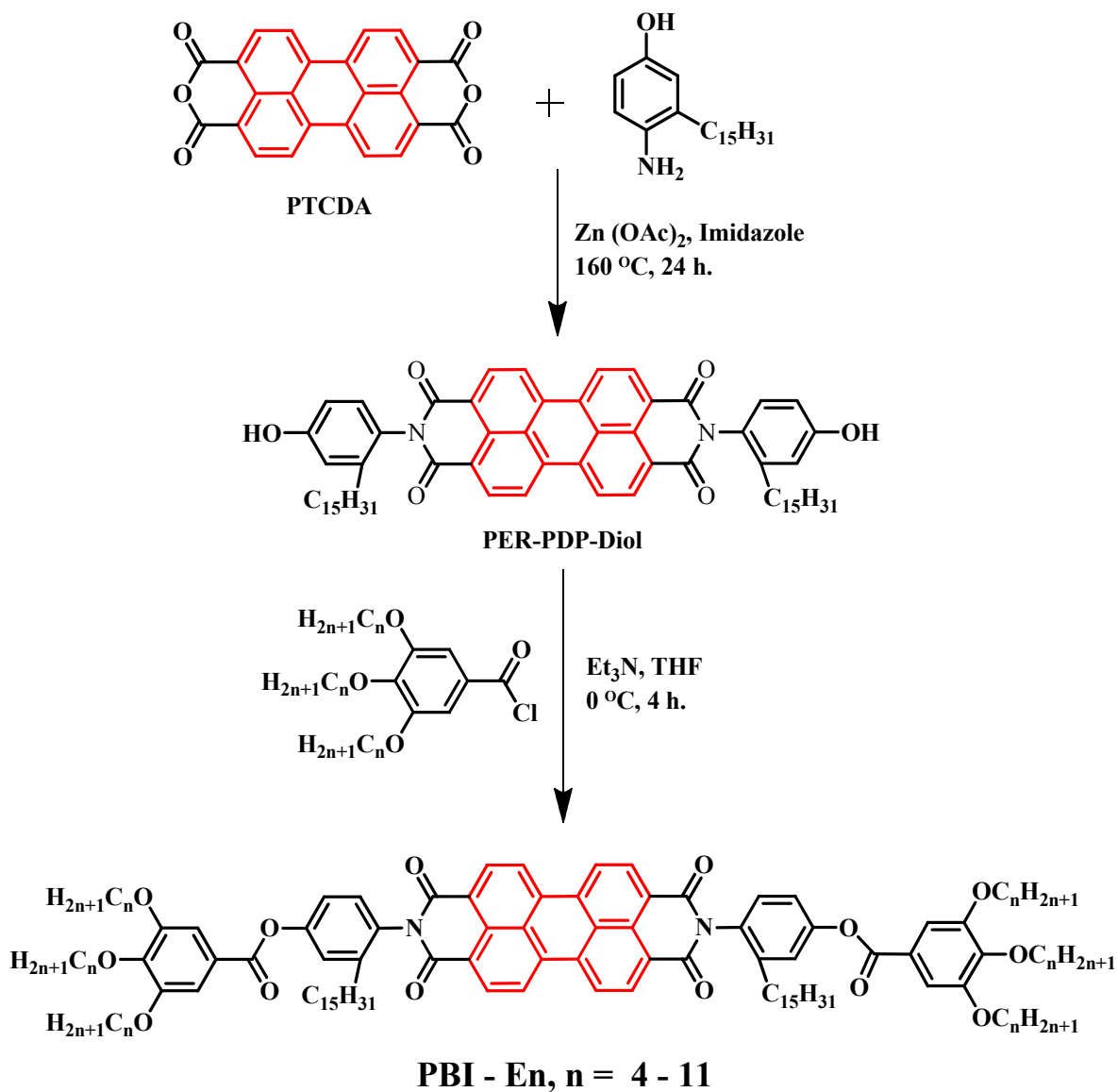
Scheme 1: Synthesis and chemical structures of PBI esters (**PBI-En**).

Figure captions

Figure 1. DSC thermograms of the **PBI-En** molecules in the second (a) heating and (b) cooling cycle at $10^{\circ}\text{C}/\text{min}$.

Figure 2. Odd–Even oscillations in the (a) clearing and the crystallization enthalpies and (b) clearing and the crystallization temperatures of **PBI-En** molecules as a function of number of carbon atoms in the terminal tri alkoxy spacer unit.

Figure 3. Polarized Light microscopic images of **PBI-En** molecules (under crossed polarizer) at room temperature. a) **PBI-E4** b) **PBI –E5** c) **PBI –E6** d) **PBI –E7** e) **PBI –E8** f) **PBI-E9** g) **PBI –E10** h) **PBI – E11** and i) **PBI – E12**.

Figure 4. Variable temperature wide angle X-ray diffraction patterns of liquid crystalline **PBI-En** molecules (a) **PBI-E8**; b) **PBI-E9**; c) **PBI-E10** and d) **PBI-E11**.

Figure 5. Wide angle X-ray diffraction pattern of annealed samples of **PBI-En** molecules from $2\theta = 5\text{--}30^{\circ}$.

Figure 6. Double logarithmic plot of the current density (J) versus applied voltage (V) measured for the **PBI-En** molecules at room temperature (25°C) in devices with area of 0.10cm^2 and thickness of $10\ \mu\text{m}$. The drop cast sample films were annealed above their clearing temperature for 20 minutes and cooled to room temperature before the measurement.

Figure 1: DSC thermograms of the **PBI-En** molecules in the second (a) heating and (b) cooling cycle at 10 °C /min.

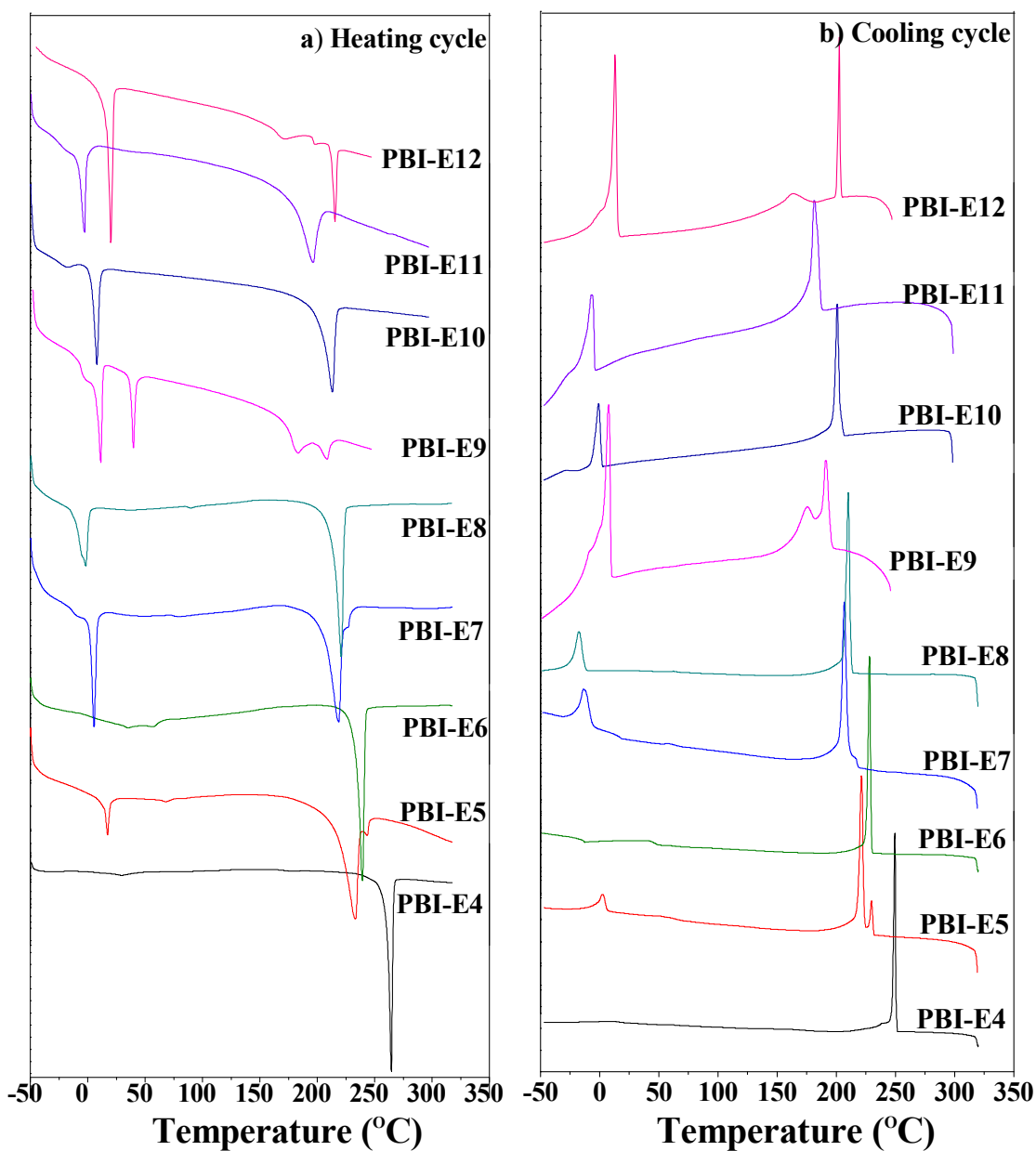


Figure 2: Odd–Even oscillations in the (a) clearing and the crystallization enthalpies and (b) clearing and the crystallization temperatures of **PBI-En** molecules as a function of number of carbon atoms in the terminal tri alkoxy spacer unit.

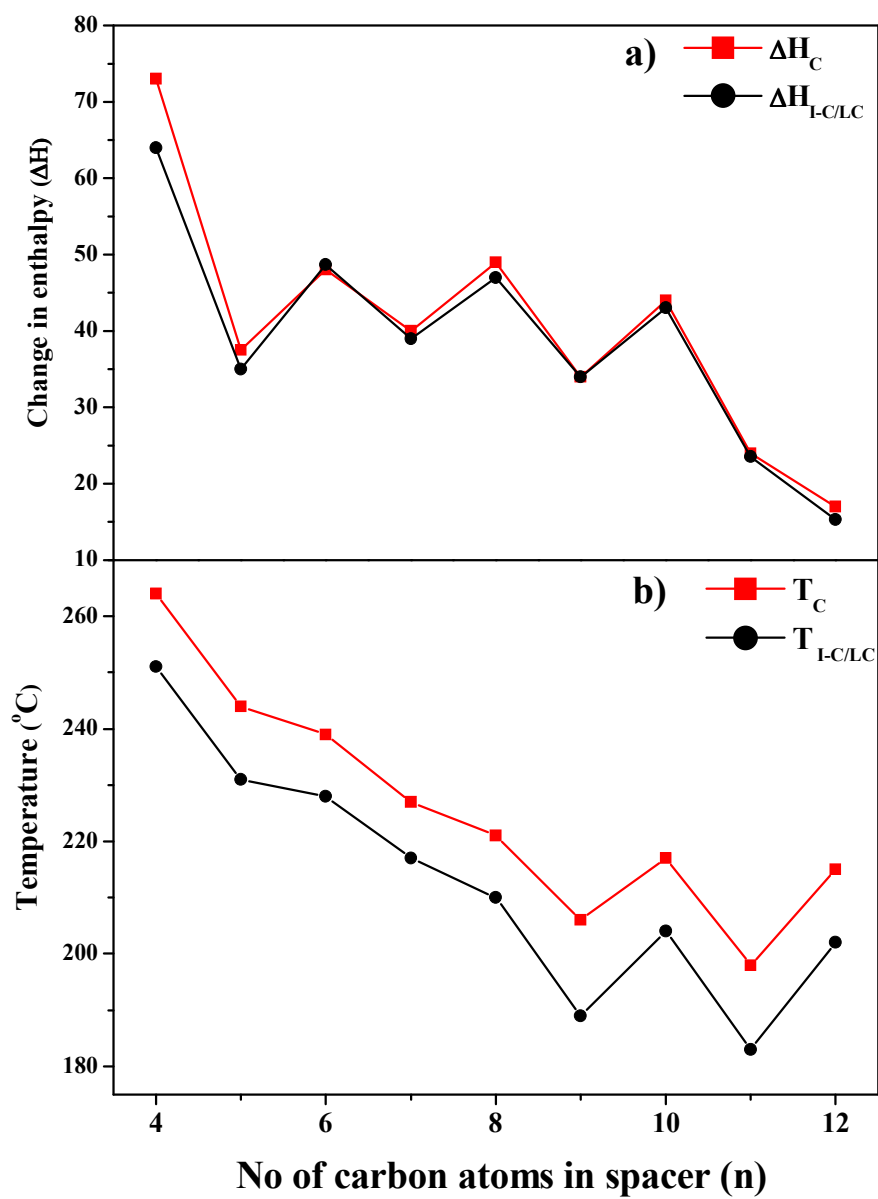


Figure 3: Polarized Light microscopic images of PBI-En molecules (under crossed polarizer) at room temperature. a) PBI-E4 b) PBI –E5 c) PBI –E6 d) PBI –E7 e) PBI –E8 f) PBI-E9 g) PBI –E10 h) PBI – E11 and i) PBI – E12.

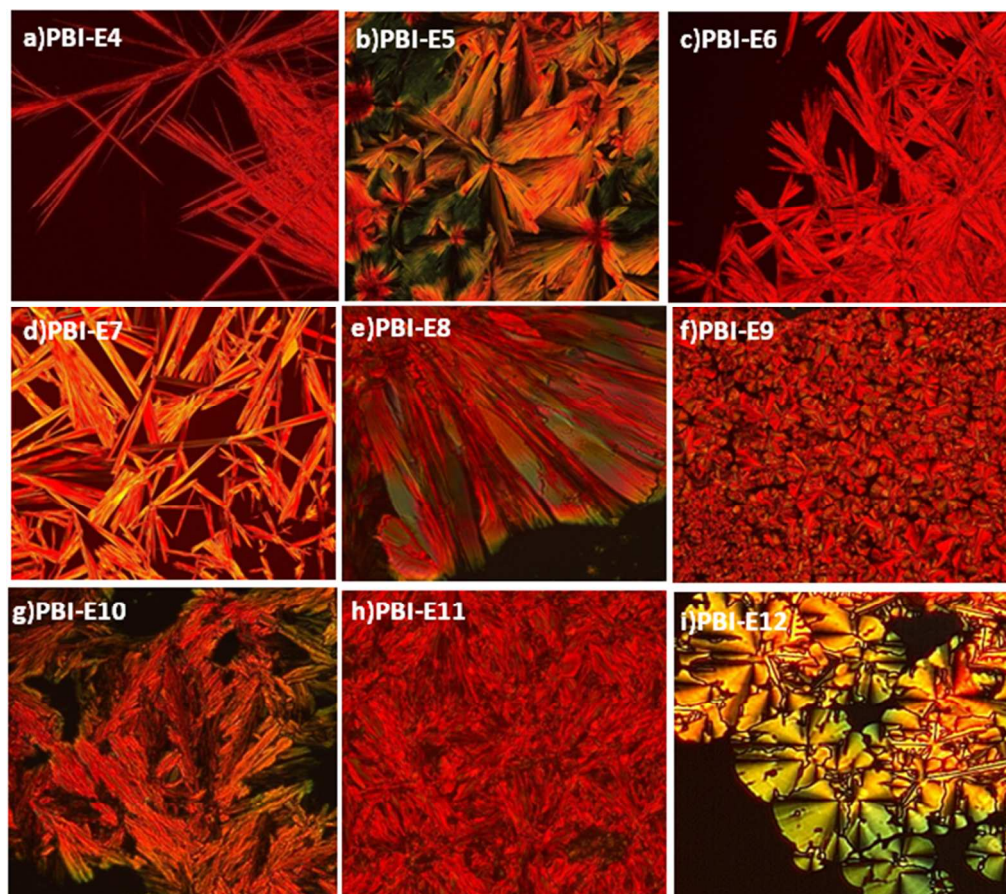


Figure 4. Variable temperature wide angle X-ray diffraction patterns of liquid crystalline PBI-En molecules (a) **PBI-E8**; b) **PBI-E9**; c) **PBI-E10** and d) **PBI-E11**.

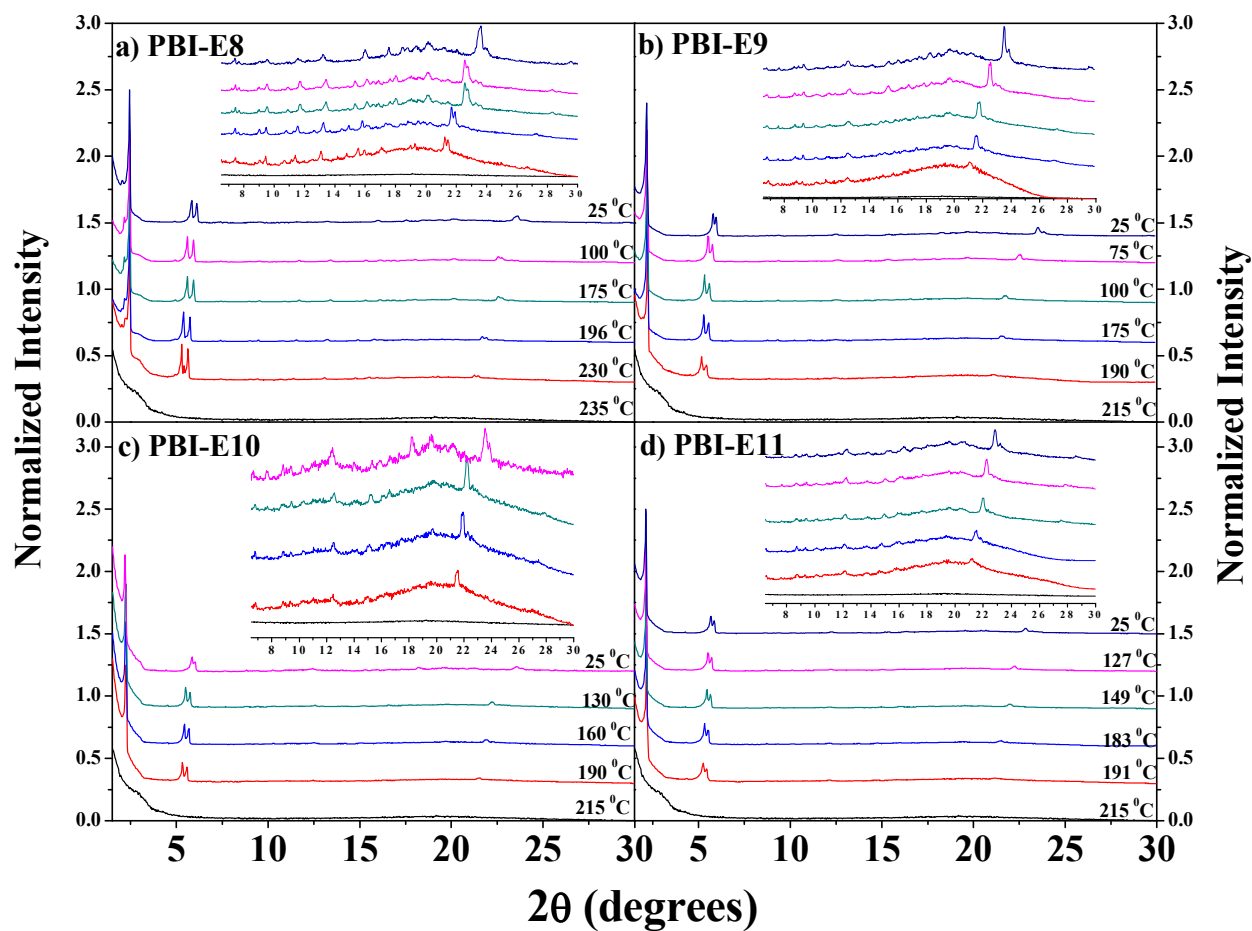


Figure 5. Wide angle X-ray diffraction pattern of annealed samples of **PBI-En** molecules from $2\theta = 5-30^\circ$.

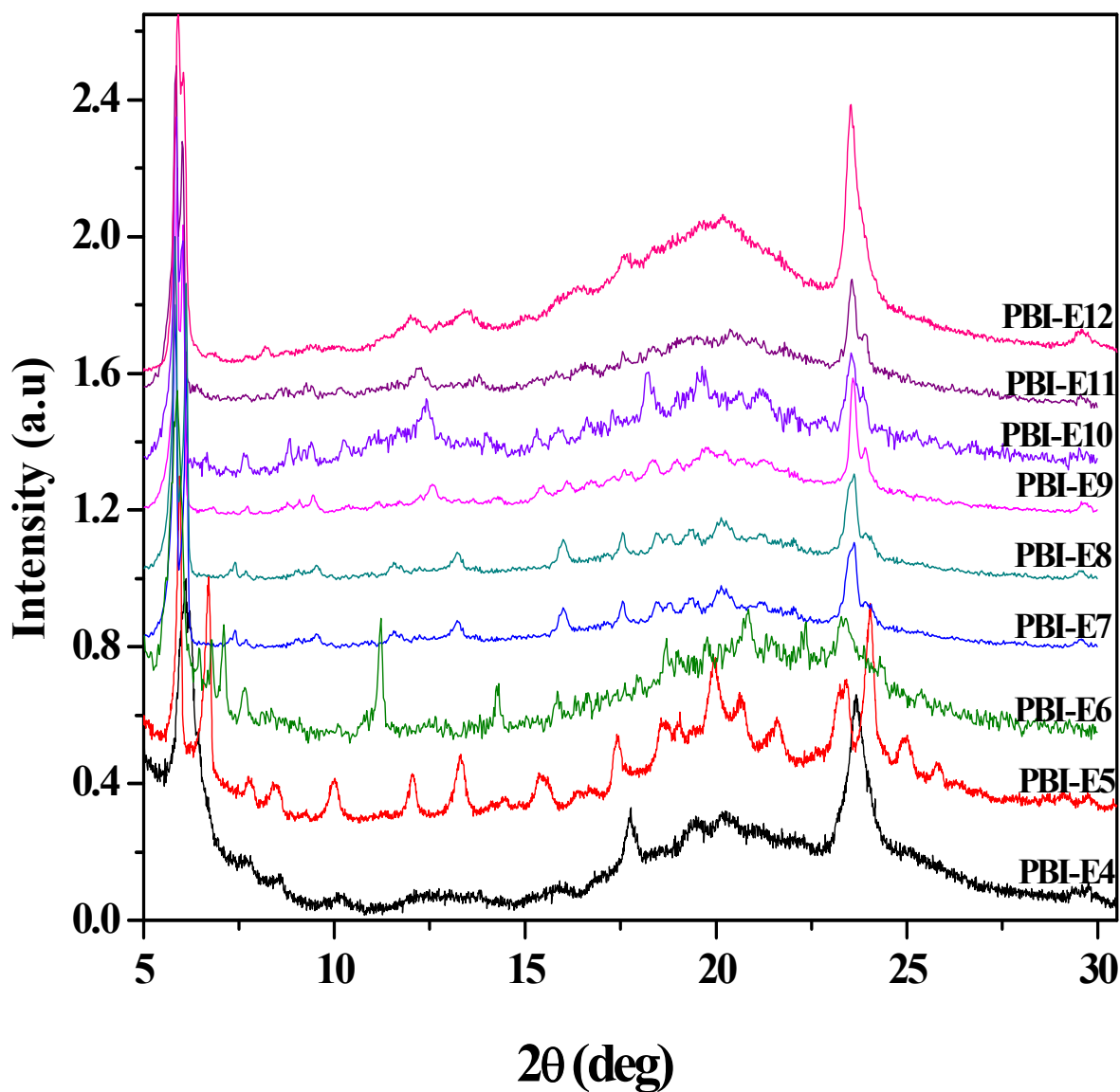


Figure-6: Double logarithmic plot of the current density (J) versus applied voltage (V) measured for the **PBI-E_n** molecules at room temperature (25 °C) in devices with area around 0.08 – 0.12 cm² and thickness of 10 μm. The drop cast sample films were annealed above their clearing temperature for 20 minutes and cooled to room temperature before the measurement.

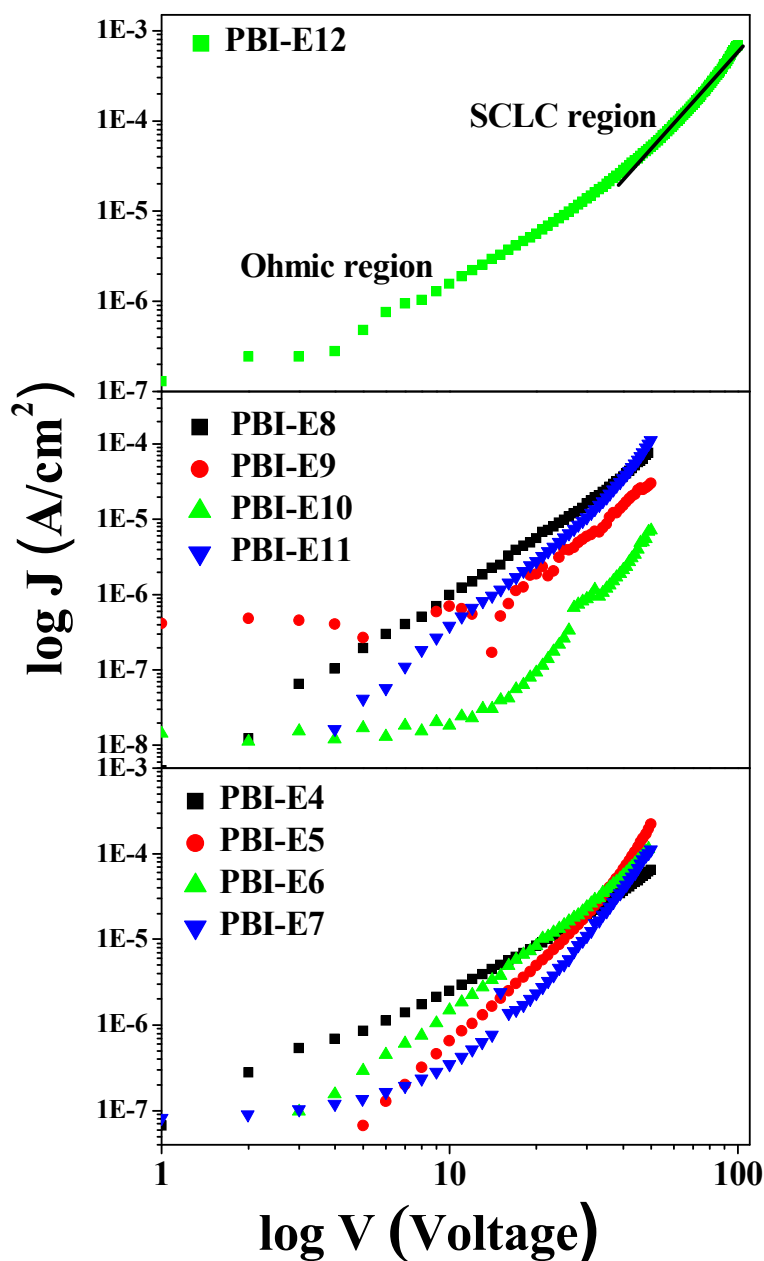


Table of Contents (TOC)Revised Manuscript submitted to *Journal of Materials Chemistry C*

Structure -Property Relationship in Charge Transporting Behaviour of Room Temperature Liquid Crystalline Perylenebisimides.

K. P. Prajitha,^{a,b} S. Chithiravel,^a K. Krishnamoorthy^{*a,b,c} and S. K. Asha^{*a,b,c}